arXiv:cond-mat/0504536v2 [cond-mat.mtrl-sci] 16 Sep 2005

Experimental demonstration of sub-wavelength image channeling using a capacitively loaded wire medium

Pekka Ikonen[1], Pavel Belov[2,3], Constantin Simovski[1,3], and Stanislav Maslovski[1]
[1] *Radio Laboratory/SMARAD, Helsinki University of Technology, P.O. Box 3000, FI-02015 TKK, Finland*
[2] *Queen Mary College, University of London, Mile End Road, London, E1 4NS, United Kingdom*
[3] *Photonics and Optoinformatics Department, St. Petersburg State University of Information Technologies, Mechanics and Optics, Sablinskaya 14, 197101, St. Petersburg, Russia*

In this letter we experimentally demonstrate a possibility to achieve significant sub-wavelength resolution of a near-field image channeled through a layer of an electromagnetic crystal. An image having radius of $\lambda/10$ has been realized using an electrically dense lattice of capacitively loaded wires. The loading allows to reduce the lattice period dramatically so that it is only a small fraction of the free-space wavelength. It is shown that losses in the structure only decrease the total amplitude of the image, but do not influence the resolution.

PACS numbers: 78.20.Ci, 42.70.Qs, 41.20.Jb

It was theoretically shown by Notomi [1] and experimentally proven by Parimi et. al [2] that in photonic crystals (PC) or electromagnetic crystals (EC) negative refraction can be achieved at frequencies close to the electromagnetic band-gap edges. Developing this direction of studies, Luo et. al. introduced a flat *superlens* formed by a slab of PC in [3], and studied theoretically the possibility for sub-wavelength imaging in a layer of EC [4]. Recently, it has been shown that with PC/EC based structures neither negative refraction or surface plasmon excitation is required to obtain a point source image whose size is smaller than $\lambda/2$. In this case the subwavelength image size has theoretically been achieved when the crystal iso-frequency contour has a special (flat) shape [5, 6, 7, 8, 9]. In this letter we experimentally validate the recently proposed concept of *sub-wavelength image channeling* [9] that explains the aforementioned effect by a transformation of evanescent modes into propagating crystal eigenmodes, and describes a special regime for the wave propagation. This regime has been called in the literature as *self collimation* [5], *directed diffraction* [6], *tunneling* [7], *absolute negative refraction* [8], and *self-guiding* [10]. In subwavelength image channeling the crystal slab effectively operates as a transmission device transferring the near field distribution of a source from the front interface to the back interface. It is conceptually important to note that the slab is not a lens in the optical point of view, and that no focusing is incorporated to the phenomenon. When the slab operates within the channeling regime and the source is located close to the front interface, the evanescent free-space harmonics transform into propagating crystal eigenmodes at the first crystal interface [9]. The near field distribution of the source is carried by these eigenmodes to the back interface where it diffracts into the free space. Very close to the back interface the channeled distribution can be detected.

The crystal structures used to theoretically demonstrate the sub-wavelength image channeling include lattices of dielectric rods [5, 7] and lattices of metal rods coated with high-permittivity dielectrics [8]. We propose to utilize *capacitively loaded wire medium* (CLWM) [11] for implementing the operational regime, see Fig. 1.a. Compared to conventional wire medium [12] or lattices of dielectric rods, CLWM offers additional features which make it superior in design. Authors of [11] have shown that CLWM has a band-gap near the resonant frequency of a single capacitively loaded wire (the so called *resonant band-gap*). By changing the value of the load capacitance, the location of this band-gap can be conveniently tuned. Moreover, high value of capacitance allows to locate the resonant band-gap significantly below the first lattice resonance, thus the needed regime can be achieved with an electrically dense lattice. Obviously, the image size is restricted by the lattice period, thus, the more (electrically) dense is the lattice, the smaller can be the image size (compared to the wavelength in free space).

For implementing the proposed regime we use the following geometry and structural dimensions (see Fig. 1): The lattice period $a = 10$ mm, the radius of wires $r_0 = 0.058a$, the insertion period for the loads $c = 2.2a$, and loading capacitance $C_0 = 0.5$ pF. The crystal sample has dimensions $N_l = 14$ and $N_t = 21$, where N_l is the number of rows of wires, and N_t is the number of

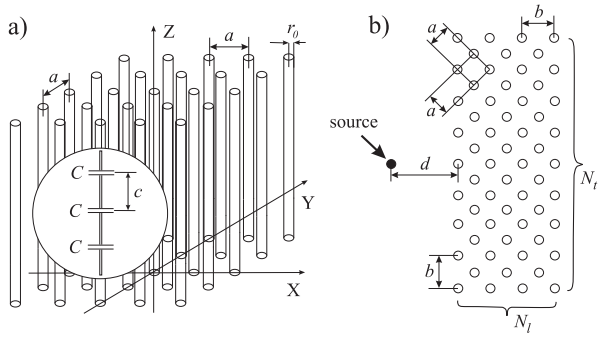


FIG. 1: a) Geometry of capacitively loaded wire medium (CLWM). b) Geometry of the crystal sample.

columns of wires. $N_l = 14$ is chosen to meet Fabry-Pérot resonance (FPR) condition at the normalized frequency $ka = 0.46$ [9], where k is the wave number in free space ($a/\lambda = 0.073$). Fig. 2.a shows isofrequency contours for the frequency region near the lower edge of the resonant band-gap. The isofrequency contour of the host matrix for $ka = 0.46$ is shown as the small circle around Γ point. The part of the isofrequency contour of the crystal corresponding to $ka = 0.46$, and located within the first Brillouin zone is practically flat. This part is perpendicular to the diagonal of the first Brillouin zone. Thus, in order to achieve channeling regime we orient interfaces of the slab orthogonally to (11)–direction of the crystal as shown in Fig. 1.b. Fig. 2.b depicts the simulated intensity distribution when using a line source as excitation [9]. There is a clear channel through the slab indicating the propagation of the excited crystal eigenmodes. A bright spot having a radius of $\lambda/6$ (determined from the intensity distribution at level max(intensity)/2) is seen in the image area.

Fig. 3.a shows a photograph of the implemented CLWM sample. To ease the fabrication, the capacitively loaded wires are implemented as printed strips on top of FR4–substrate (relative permittivity $\epsilon_r \sim 4.5(1 - j0.01)$, thickness of the plates is 1.0 mm). According to numerical simulations, losses introduced by the rather low quality substrate are within an acceptable range. Thus, despite the lowered transmission level at the desired FPR, the achieved intensity distribution should be only moderately disturbed. To implement the desired distributed capacitance level we utilize the structure shown in Fig. 3.b. Since the transverse thickness of the structure (strip) is very small, the incoming wave sees the structure as a continuous $C-$loaded strip. Also, in this structure the capacitance is well distributed along the strip leading to highly uniform current distribution. Estimated dimensions for the structure to produce the desired distributed capacitance level of 11 fF·m are $l = 22.0$ mm, $t = 0.575$ mm, and $w = 1.1$ mm (see Fig. 3.b).

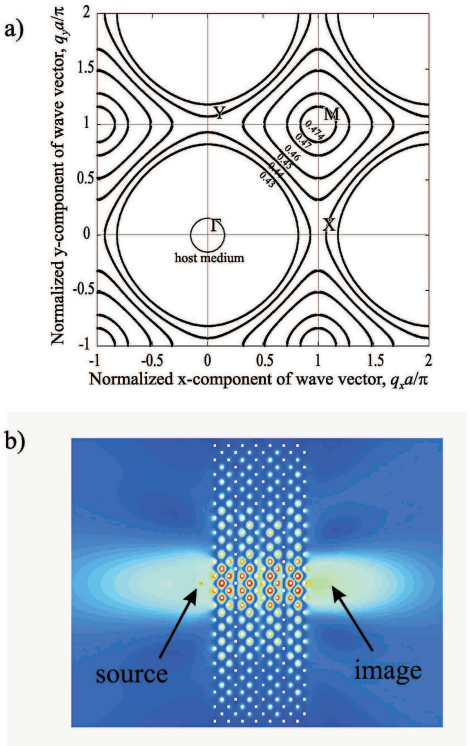


FIG. 2: a) Isofrequency contours for CLWM. The numbers correspond to values of normalized frequency ka. b) Simulated intensity distribution.

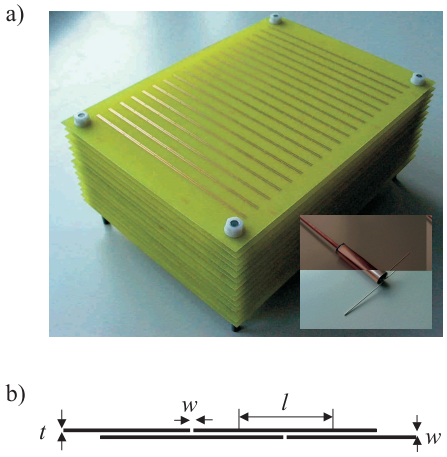


FIG. 3: a) The implemented CLWM crystal sample and the probe used in the measurements. b) A schematic illustration of the loaded wire (piece of it).

The measurement setup is schematically depicted in Fig. 4.a. The source and the probe used to scan the field distribution are connected to a vector network analyzer (VNA). The probe holder is connected to a control box responsible for the movement of the probe. VNA contains an in-house program for recording electric field values. To maximize the sensitivity of the measurement setup, the source and the probe are both based on resonant dipoles operating at the measured FPR (see Fig. 3.a for a photograph of the probe). Fig. 4.b shows the measurement areas, and the orientation of the CLWM crystal during the measurements. The spatial step of the probe is 5 mm.

First, we need to locate the desired FPR for which the slab has been tuned. This frequency lies approximately at the lower edge of the first crystal stop band. To locate the FPR we measure the reflection level from the slab using a wide-band horn. The result is presented in Fig. 5. Undoubtedly, there are strong near field interactions between the slab and the horn so Fig. 5 does not properly show the true reflection properties of the slab. Nevertheless, the stop band edge at 1.73 GHz, and the FPR at 1.684 GHz are seen in Fig. 5: only a traveling

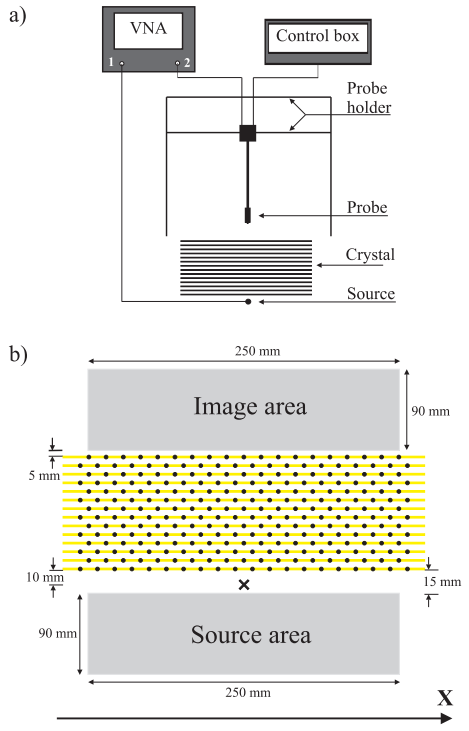


FIG. 4: a) A schematic illustration of the measurement setup. b) The measurement area. The black dots denote the loaded strips, the cross denotes the source.

wave is capable of producing the resonant peaks shown in Fig. 5. Inside the stop-band of the structure a wave decays exponentially and the amplitude of the reflection coefficient approaches unity. Thus, when the resonant peaks are not anymore seen and the reflection coefficient amplitude is close to unity we have found the stop-band edge.

The dielectric plates have a visible influence on the transmission characteristics: the lower edge of the resonant stop band has shifted from the predicted (for wires in free space) 2.20 GHz [9] to 1.73 GHz. Consequently,

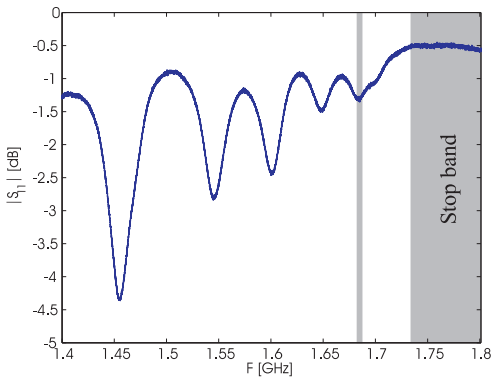


FIG. 5: Measured $S_{11}-$level of the slab. The desired Fabry-Pérot resonance is shown with a vertical line.

there is most likely some discrepancy in the estimated parameters used to predict the capacitance level. From the measured location of the lower stop band edge we estimate that effectively the distributed capacitance level at the FPR is 17.6 fF·m. According to the numerical simulations higher capacitance level should improve the resolution.

The following measurements have been performed at frequency 1.684 GHz which corresponds to the FPR identified from the reflection measurement. Fig. 6.a shows the measured intensity distribution in the source and the image area. We can observe that there is a clear and symmetrical image at the predicted image location. The radius of the image (determined at level max(intensity)/2) is approximately 0.10λ, thus we are dealing with a significant sub-wavelength resolution. It is worth noticing that due to the nature of the measurement probe, the probe is inherently incapable of averaging the detected transmitted field (as is the case e.g. with loop detectors [13]). Since the dipole arm is very thin, the exact dis-

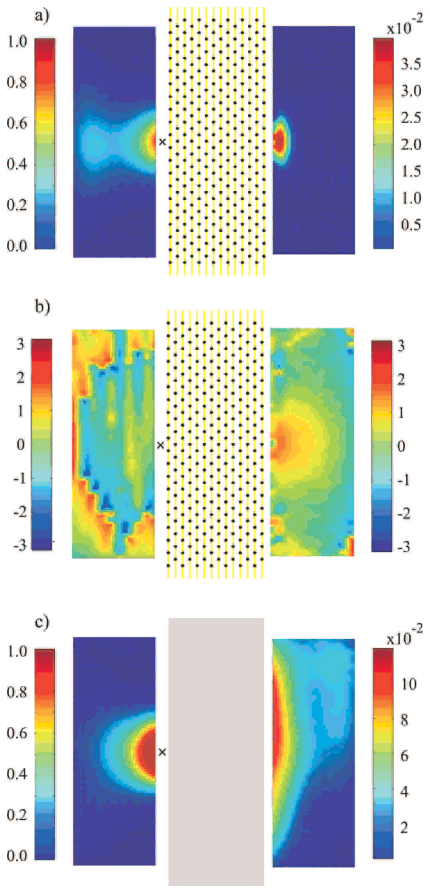


FIG. 6: a) The measured intensity distribution (in arb. units). b) The measured phase distribution of electric field (in radians). c) The measured intensity distribution without the CLWM crystal (in arb. units). In a) and c) the intensity values in the image area have not been normalized to better see the details of the intensity distribution.

tribution of the transmitted field can be very accurately measured, and the resolution of the image hardly depends on the electrical size of the probe. Contrary to the simulations, we can observe from Fig. 6.a that as the probe moves closer to the slab interface, the field strength slightly decreases. This is most likely caused by destructive interaction between the metal parts of the probe and the metal strips leading to the loss of the resonant condition in the vicinity of the wire surface (similar effect has been observed with loop shaped metal particles and loop shaped metal detector [13]).

The measured phase distribution of the electric field is presented in Fig. 6.b. In the image area we can identify the phase front of a wave diverging from the image. In the source area the phase distribution is disturbed by reflections from the slab. Fig. 6.c shows the measured intensity distribution without the crystal (the shadowed region shows the space previously occupied by the slab). Slight asymmetry is seen in the cylindrical intensity profile. This weak asymmetry is expected to be caused by parasitic currents induced to the balun of the source probe (the transversal thickness of the balun is not negligible). The effect of parasitic radiation is not seen in the source area when the field level produced by the dipole radiation is strong. Moreover, the parasitic radiation does not destroy the symmetry of the intensity profile when the slab is present. This is due to the fact that outside the channel the field level is very low (most of the energy flows inside the channel), thus the parasitic radiation directed away from the symmetry axis of the slab attenuates rapidly before approaching the image area.

The measured transversal intensity distributions are shown in Fig. 7 (see Fig. 4.b for definition of the coordinate system). The measured maximum field value is approximately 35 percent lower when using the crystal slab than in the free space measurement. The biggest reason for this degradation is the strong reflection occurring at the first crystal interface. The lossy dielectric plates also degrade the amplitude level of the channeled field. It is important to note, however, that the image shape is not affected by the losses. This important practical property is inherent to the subwavelength image channeling: the propagating waves in a lossy material experience the same decay irrespective of their transversal wave vector components which are responsible for the shape of the image.

In the present letter we have experimentally validated the concept of sub-wavelength image channeling using a slab of an electromagnetic crystal. It has been shown that losses influence only to the total amplitude of the image, but do not disturb its shape. We have shown that an image with radius of $\lambda/10$ can be achieved using an electrically dense lattice of capacitively loaded wires. The image size is noticeably below the theoretical diffraction limit, and it is twice smaller than the minimum image size practically obtained in the modern high-precision microscopy. Compared to the results obtained in the optical regime [14] the quality of imaging is improved twice. In the microwave regime the proposed structure could be used as a wave channel multiplexer or a decoupler for antenna systems.

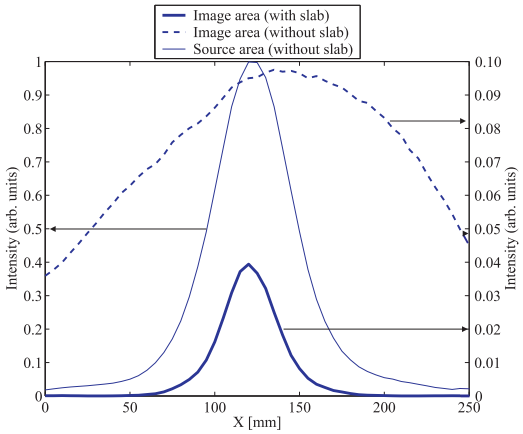


FIG. 7: Measured intensity distribution along the axis X (parallel to the slab interface). The arrow indicates the scale which is used to read the intensity values. Intensity in the image area has been measured at 10 mm distance from the slab interface. Intensity in the source area has been measured at 10 mm distance from the source.

Useful discussions with Prof. Sergei Treyakov are acknowledged. One of the authors (P.I.) wishes to thank Mr. Eino Kahra from the Radio Laboratory TKK for assistance in manufacturing the prototype.

[1] M. Notomi, Phys. Rev. B **62**, 10696 (2000).
[2] P. V. Parimi, W. T. Lu, P. Vodo, and S. Sridhar, Nature **426**, 404 (2003).
[3] C. Luo, S. G. Johnson, J. Joannopoulos, and J. Pendry, Phys. Rev. B **65**, 201104 (2002).
[4] C. Luo, S. G. Johnson, J. Joannopoulos, and J. Pendry, Phys. Rev. B **68**, 045115 (2003).
[5] Z.-Y. Li and L.-L. Lin, Phys. Rev. B **68**, 245110 (2003).
[6] H.-T. Chien, H.-T. Tang, C.-H. Kuo, C.-C. Chen, and Z. Ye, Phys. Rev. B **70**, 113101 (2004).
[7] C.-H. Kuo and Z. Ye, Phys. Rev. E **70**, 056608 (2004).
[8] X. Zhang, Phys. Rev. B **70**, 205102 (2004).
[9] P. A. Belov, C. R. Simovski, and P. Ikonen, Phys. Rev. B. **71**, 193105 (2005).
[10] D. N. Chigrin, S. Enoch, C. M. S. Torres, and G. Tayeb, Optics Express **11**, 1203 (2003).
[11] P. Belov, C. Simovski, and S. Tretyakov, Phys. Rev. E **66**, 036610 (2002).
[12] N. Nicorovici, R. McPhedran, and L. Botten, Phys. Rev. E **52**, 1135 (1995).
[13] R. Marqués, F. Martín, and M. Sorolla, Proc. Latsis Symposium pp. 50–53 (2005).
[14] N. Fang, H. Lee, C. Sun, and X. Zhang, Science **308**, 534 (2005).